iScience

CellPress
OPEN ACCESS

Article

Chronic modulation of cAMP signaling elicits synaptic scaling irrespective of activity

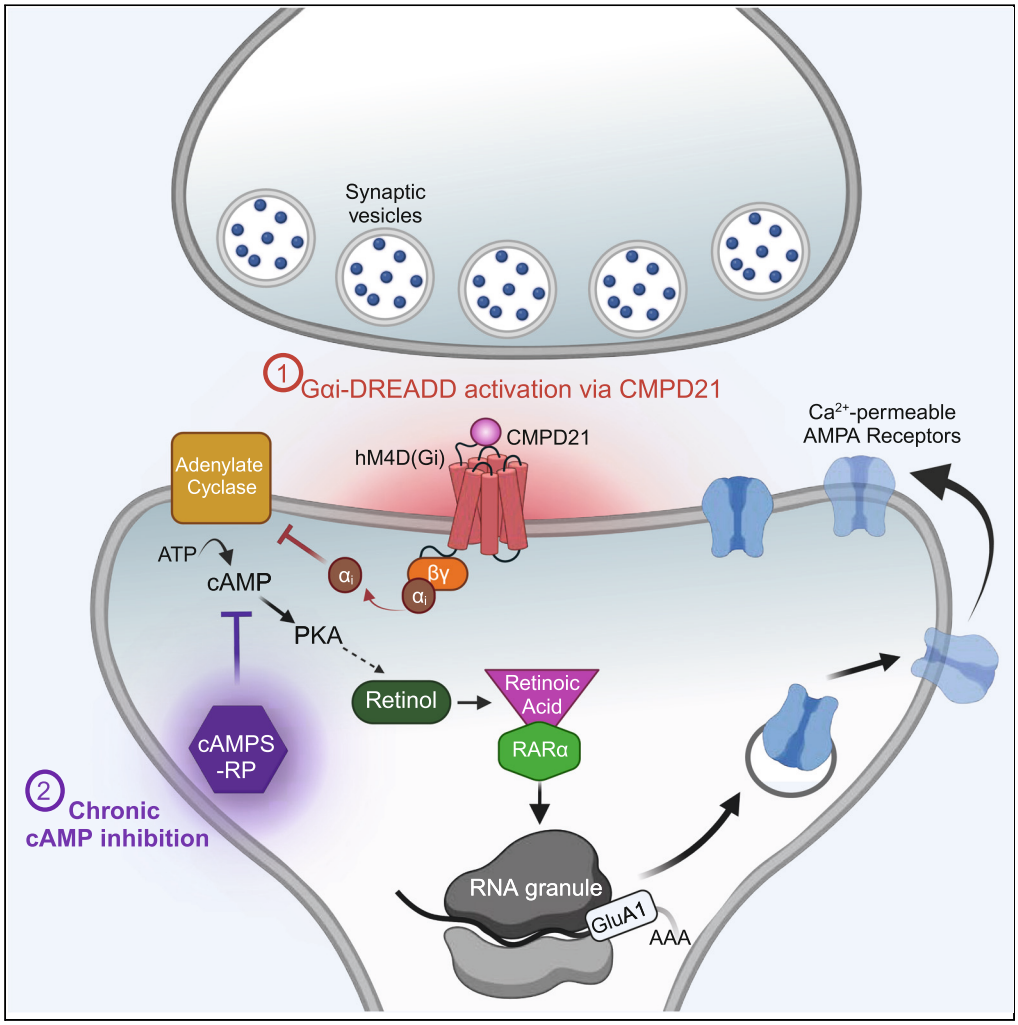

Elena D. Bagatelas, Ege T. Kavalali

ege.kavalali@vanderbilt.edu

Highlights

Modulation of Gαi-signaling prompts homeostatic plasticity irrespective of activity

This activity-independent homeostatic plasticity converges on the RARα pathway

Homeostatic synaptic upscaling by Gαi-signaling operates in a cell-autonomous manner

Gαi-signaling-driven homeostatic synaptic plasticity relies on insertion of CP-AMPARs

Bagatelas & Kavalali, iScience *27*, 110176
July 19, 2024
https://doi.org/10.1016/j.isci.2024.110176

iScience

CellPress
OPEN ACCESS

Article

Chronic modulation of cAMP signaling elicits synaptic scaling irrespective of activity

Elena D. Bagatelas[1] and Ege T. Kavalali[1,2,*]

SUMMARY

Homeostatic plasticity mechanisms act in a negative feedback manner to stabilize neuronal firing around a set point. Classically, homeostatic synaptic plasticity is elicited via rather drastic manipulation of activity in a neuronal population. Here, we employed a chemogenetic approach to regulate activity via eliciting G protein-coupled receptor (GPCR) signaling in hippocampal neurons to trigger homeostatic synaptic plasticity. We demonstrate that chronic activation of hM4D(Gi) signaling induces mild and transient activity suppression, yet still triggers synaptic upscaling akin to tetrodotoxin (TTX)-induced complete activity suppression. Therefore, this homeostatic regulation was irrespective of Gi-signaling regulation of activity, but it was mimicked or occluded by direct manipulation of cyclic AMP (cAMP) signaling in a manner that intersected with the retinoic acid receptor alpha (RARα) signaling pathway. Our data suggest chemogenetic tools can uniquely be used to probe cell-autonomous mechanisms of synaptic scaling and operate via direct modulation of second messenger signaling bypassing activity regulation.

INTRODUCTION

Detection of chronic changes in activity is thought to be a key factor for neurons to adjust synaptic strength across all synapses to sustain neuronal excitability within a dynamic range. Unlike traditional Hebbian plasticity, which is activity dependent and relatively input specific for promoting synaptic strength, homeostatic plasticity orchestrates dynamic widespread scaling across a neuronal network while maintaining the relative strength of synapses in a bidirectional manner. By restoring a neuron to its set point, the system remains not only stable but also adaptive to plasticity and degeneration, serving a crucial role in neurodevelopment, synaptic transmission, and network dynamics.[1–3] Currently, most of the work probing cellular mechanisms underlying homeostatic plasticity at the synapse relies on *in vitro* manipulations; therefore, the processes that regulate scaling in an intact brain may differ from observations in more reduced systems. Nevertheless, as deficits in homeostatic plasticity have been reported in a variety of mood and neurodevelopmental disorders, there is a need to unveil pathways mediating homeostatic plasticity mechanisms to explore potential therapeutic targets.[4]

Previous efforts to probe homeostatic synaptic plasticity have relied on pharmacological manipulation to simulate low activity environments; however, the complete suppression of activity in a network does not correlate to *in vivo* activity. Thus, chemogenetic manipulation is an alternative to surgically perturb environmental conditions in a cell-autonomous manner and probe signaling mechanisms that maintain synaptic homeostasis. Here, we show that use of hM4D(Gi)-designer receptors activated only by designer drugs (DREADDs) can initiate homeostatic synaptic upscaling without fully suppressing neuronal activity. Instead, we found that chronic hM4D(Gi) activation results in synaptic scaling via the retinoic acid receptor alpha (RARα)-dependent signaling pathway in an activity-independent manner. We elucidate how this pathway can be triggered in parallel by chronic blockade of cyclic AMP (cAMP) activity to elicit synaptic upscaling through direct modulation of Gαi-signaling factors. We also uncovered how this synaptic upscaling requires recruitment of calcium-permeable α-amino-3-hydroxy-5-methyl-4-isoxazolepropionic acid glutamate receptors (CP-AMPARs). This study reveals downstream implications for G protein-dependent second messenger cascades as targets for regulating synaptic scaling amid an environment with diverse signaling.

RESULTS

Compound 21 selectively acts on DREADD-expressing neurons

We investigated signaling pathways underlying multiplicative synaptic scaling mechanisms with the expression of inhibitory hM4D(Gi)-DREADDs in primary hippocampal neuronal cultures. Earlier studies have successfully used DREADDs to manipulate activity in a chronic fashion,[5] which prompted us to utilize chemogenetics for studying molecular mediators of homeostatic plasticity in our system. To demonstrate the successful expression of our DREADD of interest (hSyn-hM4D(Gi)-mCherry or hSyn-EV-mCherry), we visualized the DREADD (mCherry) expression superimposed on MAP2 staining (GFP) (Figures 1A and 1B). Our Gi-DREADD is neuron specific, and our focus is on excitatory transmission; therefore, we first investigated whether DREADD activity alters action potentials and spontaneous activity in

[1]Department of Pharmacology and the Vanderbilt Brain Institute, Vanderbilt University, Nashville, TN 37209, USA
[2]Lead contact
*Correspondence: ege.kavalali@vanderbilt.edu
https://doi.org/10.1016/j.isci.2024.110176

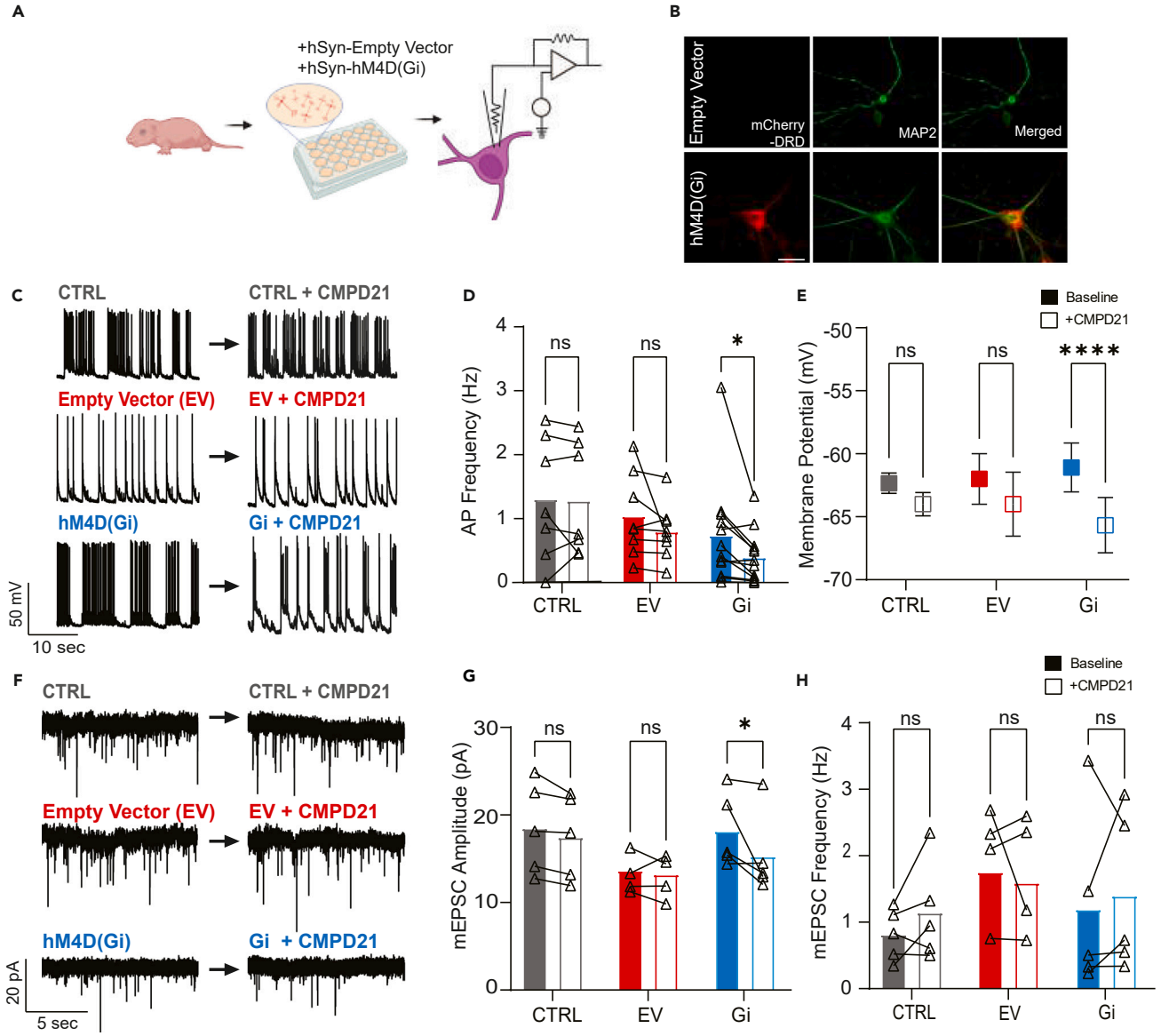

Figure 1. Compound 21 selectively acts on DREADD-expressing neurons

(A) Experimental design. Lentiviral constructs were transfected on DIV 4 with virus carrying hM4D(Gi) or Empty Vector, and experiments were performed between DIV 14–21.

(B) Representative images of immunostaining for mCherry-DREADD and MAP2 staining. Representative scale bar, 20 μm.

(C) Representative current-clamp traces of spontaneous firing before (left) and after (right) acute 1 μM CMPD21 perfusion on control (CTRL), empty vector (EV), and hM4D(Gi) neurons.

(D) Comparison of the mean action potential frequency (Hz) following CMPD21 wash (two-way ANOVA with Sidak's multiple comparisons test, CTRL vs. CTRL + CMPD21 $p = 0.889$; EV vs. EV + CMPD21 $p = 0.150$; Gi vs. Gi + CMPD21 $p = 0.015$; $N = 2–3$, $n = 7–12$ per group).

(E) Comparison of mean resting membrane potential (mV) (two-way ANOVA with Sidak's multiple comparisons test, CTRL vs. CTRL + CMPD21 $p = 0.276$; EV vs. EV + CMPD21 $p = 0.053$; Gi vs. Gi + CMPD21 $p < 0.0001$; $N = 2–3$, $n = 7–12$ per group).

(F) Representative raw traces of AMPA-mediated mEPSCs before (left) and after (right) acute 1 μM CMPD21 perfusion.

(G) Comparison of the mean mEPSC amplitude (pA) following CMPD21 wash (two-way ANOVA with Dunnett's multiple comparisons test, CTRL baseline vs. CTRL + CMPD21 $p = 0.697$; EV baseline vs. EV + CMPD21 $p = 0.990$; Gi baseline vs. Gi + CMPD21 $p = 0.043$; $N = 2–3$, $n = 5–6$ per group).

(H) Comparison of the mean mEPSC frequency (Hz) following CMPD21 wash (two-way ANOVA with Dunnett's multiple comparisons test, CTRL baseline vs. CTRL + CMPD21 $p = 0.728$; EV baseline vs. EV + CMPD21 $p = 0.888$; Gi baseline vs. Gi + CMPD21 $p = 0.913$; $N = 2–3$, $n = 5–6$ per group). Data are represented as mean ± SEM. Significant symbols used in figures are defined as such: $*p < 0.05$; $**p < 0.01$; $***p < 0.001$; n.s.

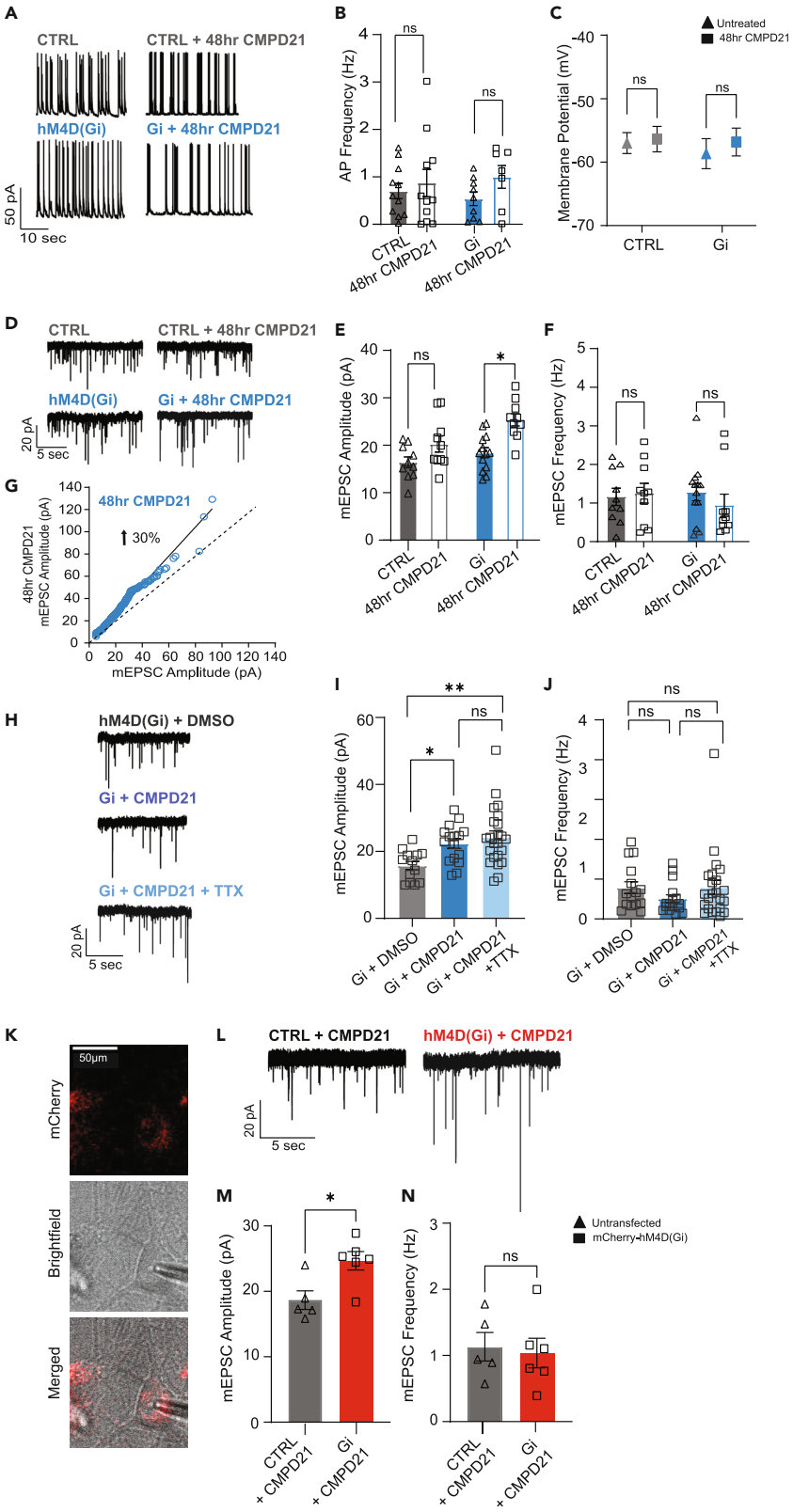
A
CTRL
CTRL + 48hr CMPD21
hM4D(Gi)
Gi + 48hr CMPD21
50 pA
10 sec
B
AP Frequency (Hz)
ns
ns
CTRL
48hr CMPD21
Gi
48hr CMPD21
C
Untreated
48hr CMPD21
Membrane Potential (mV)
ns
ns
CTRL
Gi
D
CTRL
CTRL + 48hr CMPD21
hM4D(Gi)
Gi + 48hr CMPD21
20 pA
5 sec
E
mEPSC Amplitude (pA)
ns
*
CTRL
48hr CMPD21
Gi
48hr CMPD21
F
mEPSC Frequency (Hz)
ns
ns
CTRL
48hr CMPD21
Gi
48hr CMPD21
G
48hr CMPD21
mEPSC Amplitude (pA)
48hr CMPD21
30%
mEPSC Amplitude (pA)
H
hM4D(Gi) + DMSO
Gi + CMPD21
Gi + CMPD21 + TTX
20 pA
5 sec
I
mEPSC Amplitude (pA)
**
*
ns
Gi + DMSO
Gi + CMPD21
Gi + CMPD21 +TTX
J
mEPSC Frequency (Hz)
ns
ns
ns
Gi + DMSO
Gi + CMPD21
Gi + CMPD21 +TTX
K
50μm
mCherry
Brightfield
Merged
L
CTRL + CMPD21
hM4D(Gi) + CMPD21
20 pA
5 sec
M
mEPSC Amplitude (pA)
*
CTRL + CMPD21
Gi + CMPD21
N
Untransfected
mCherry-hM4D(Gi)
mEPSC Frequency (Hz)
ns
CTRL + CMPD21
Gi + CMPD21

Figure 2. Chronic chemogenetic activity elicits synaptic upscaling in a cell-autonomous manner

(A) Representative raw current clamp traces at baseline and 48 h after 1 μM CMPD21.

(B) Comparison of the mean action potential frequency (Hz) following chronic CMPD21 (two-way ANOVA with Sidak's multiple comparisons test, CTRL vs. 48 h CMPD21 $p = 0.818$; Gi vs. 48 h CMPD21 $p = 0.347$; $N = 3$, $n = 7–11$ per group). (C) Comparison of the mean resting membrane potential (mV) following chronic CMPD21 (two-way ANOVA with Sidak's multiple comparisons test, CTRL vs. 48 h CMPD21 $p = 0.952$; Gi vs. 48 h CMPD21 $p = 0.850$; $N = 3$, $n = 7–11$ per group). (D) Representative raw voltage clamp traces at baseline and 48 h after 1 μM CMPD21.

(E) Comparison of the mean mEPSC amplitude (pA) following 48 h CMPD21 (two-way ANOVA with Sidak's multiple comparisons test, CTRL vs. 48 h CMPD21 $p = 0.085$; Gi vs. Gi + CMPD21 $p = 0.023$; $N = 2–5$, $n = 10$ per group). (F) Comparison of the mean mEPSC frequency (Hz) following 48 h CMPD21 (two-way ANOVA with Dunnett's multiple comparisons test, CTRL vs. 48 h CMPD21 $p = 0.918$; Gi vs. Gi 48 h CMPD21 $p = 0.717$; $N = 2–5$, $n = 10$ per group). (G) Rank-order plot of mEPSC amplitudes Gi + 48 h DMSO versus Gi+ 48 h CMPD21 ($y = 1.30$, $r^2 = 0.983$). (H) Representative raw voltage clamp traces at baseline, 48 h after DMSO, 1 μM CMPD21, and 48 h after 1 μM CMPD21 + 1 μM TTX.

(I) Comparison of the mean mEPSC amplitude (pA) following 48 h treatment for each condition. Some of dataset combined with previous experiments performed that underwent same procedures (two-way ANOVA with Tukey's multiple comparisons test, Gi + DMSO vs. Gi + 48 h CMPD21 $p = 0.041$; Gi + DMSO vs. Gi + 48 h CMPD21 + TTX $p = 0.003$; Gi + 48 h CMPD21 vs. Gi + 48 h CMPD21 + TTX $p = 0.679$; $N = 2–5$, $n = 13–19$ per group). (J) Comparison of the mean mEPSC frequency (Hz) following 48 h treatment for each condition (two-way ANOVA with Tukey's multiple comparisons test, Gi + DMSO vs. Gi + 48 h CMPD21 $p = 0.486$; Gi+ DMSO vs. Gi + 48 h CMPD21 + TTX $p = 0.999$; Gi + 48 h CMPD21 vs. Gi + 48 h CMPD21 + TTX $p = 0.394$; $N = 2–5$, $n = 13–19$ per group). (K) Representative images of mCherry-hM4D(Gi)-expressing neurons. (L) Representative raw voltage clamp traces of untransfected neurons and mCherry-hM4D(Gi) neurons. Representative scale bar, 50 μm. (M) Comparison of the mean mEPSC amplitude (pA) following 48 h treatment (unpaired t test, CTRL + CMPD21 vs. hM4D(Gi) + CMPD21, $p = 0.017$, N=1, $n = 5–6$ per group). (N) Comparison of the mean mEPSC frequency (Hz) following 48 h treatment (unpaired t test, CTRL + CMPD21 vs. hM4D(Gi) + CMPD21, $p = 0.792$, $N = 1$, $n = 5–6$ per group). Data are represented as mean ± SEM. Significant symbols used in figures are defined as such: $*p < 0.05$; $**p < 0.01$; $***p < 0.001$; n.s.

hippocampal neurons. While continuously recording from the same neuron, we acutely perfused 1 μM Compound 21 (CMPD21), a highly potent and selective DREADD agonist,[6–9] to assess its action on hM4D(Gi)-expressing neurons compared to control (CTRL) (wild type) and empty vector (EV)-expressing neurons (Figure 1C). Acute application of CMPD21 significantly hyperpolarized the resting membrane potential of hM4D(Gi)-expressing neurons and decreased, but not completely inhibited, action potential firing in hM4D(Gi)-expressing neurons. In contrast, the same treatment had no effect on resting membrane potential or action potential frequency of EV or CTRL neurons (Figures 1D and 1E), demonstrating CMPD21 selectivity for hM4D(Gi)-DREADD receptors in our system.

We then examined the effects of DREADDs on spontaneous neurotransmission by performing whole-cell voltage-clamp recordings and found that neurons showed a significant decrease in miniature excitatory postsynaptic current (mEPSC) amplitudes—recorded in tetrodotoxin (TTX) to block activity—following CMPD21 application, with no difference in mEPSC amplitudes for EV or CTRL neurons consistent with lack of off-target effects (Figure 1G). We observed a significant decrease in mEPSC amplitude for Gi-DREADD-expressing neurons, which suggests there may be acute off-target effects of CMPD21 on spontaneous neurotransmission in Gi-expressing neurons (but not a direct effect of cAMP signaling, see below). In addition, there was no effect of acute CMPD21 application on mEPSC frequency across all groups (Figures 1H and 1F). Since there were no observable differences between CTRL and EV groups in current or voltage-clamp experiments, we use CTRL neurons for comparison for the rest of our experiments. From our initial findings, we concluded that CMPD21 can be used for further experimentation to selectively activate hM4D(Gi)-DREADDs to chronically manipulate activity.

Chronic chemogenetic activity elicits classic synaptic upscaling

Signaling pathways that generate changes underlying homeostatic synaptic activity are triggered following prolonged external perturbations over the course of hours to days.[4,10] A homeostatic plasticity induction protocol in cultured neurons induces scaling by inhibiting network activity for 48 h via voltage-gated Na^+ channel blocker TTX application, resulting in an increase in mEPSC amplitude with no change on mEPSC frequency.[11–13] More recent studies probed homeostatic plasticity changes *in vivo* using chronic chemogenetic manipulation, where chronic hM4D(Gi)-DREADD activation elicited upscaling of mEPSC amplitudes.[5,14] Thus, we sought to investigate whether chronic DREADD activation via CMPD21 could be used to effectively study molecular mediators of homeostatic synaptic plasticity mechanisms.

We measured the effects of chronic DREADD activation using whole-cell current-clamp recordings to identify changes in neuronal properties following 48 h of 1 μM CMPD21 in the cell media (comparable timeline to canonical TTX scaling experiments) (Figure 2A). We recorded action potential activity with no CMPD21 in the bath and observed no significant changes in action potential frequency for CTRL or hM4D(Gi)-expressing neurons after 48 h treatment (Figures 2B and 2C). This result illustrates that inhibition of activity via hM4D(Gi)-DREADDs leads to rebound renormalization of action potentials and of resting membrane potential. Whole-cell voltage-clamp recordings, performed on neurons following 48 h of CMPD21, did not reveal significant changes in AMPAR-mEPSC amplitudes for CTRL cultures. Interestingly, we found a significant increase in AMPAR-mEPSC amplitudes in hM4D(Gi)-expressing neurons (Figure 2E). When mEPSC amplitudes with and without treatment were plotted in rank order, 48 h of CMPD21 activation showed a significant increase (~30%) in slope compared to the untreated group, illustrating that chronic hM4D(Gi) activation induced synaptic upscaling (Figure 2G). We did not detect any changes in mEPSC frequency in any condition after 48 h treatment, in line with previous findings from multiple groups (Figure 2F).[5,10–12,14–24]

We then tested whether the classic homeostatic scaling protocol—chronic application of TTX—would augment scaling when combined with the hM4D(Gi)-induced chemogenetic scaling approach. We did not see a significant difference between mEPSC amplitudes recorded in hM4D(Gi)-expressing neurons treated with either CMPD21 alone or CMPD21 + TTX for 48 h. However, both groups demonstrated synaptic

scaling compared to DMSO alone (Figures 2H–2J). This result illustrates that synaptic scaling via hM4D(Gi) signaling is occluded by TTX co-application, suggesting they converge onto the same pathway.

So far, our data indicate that CMPD21 can be used to chronically activate hM4D(Gi)-DREADDs in a selective manner that circumvents any off-target effects on wild-type neurons. This finding provides support for how chronic Gi-DREADD activation can trigger synaptic strengthening of AMPAR-mediated responses even during transient suppression of action potential activity. Interestingly, the level of synaptic scaling induced by Gi-DREADD activation was comparable to synaptic scaling seen after complete suppression of activity with TTX. Furthermore, hM4D(Gi)-DREADD-induced synaptic scaling was occluded by concomitant TTX-induced scaling.

Utilizing Gi-signaling to selectively trigger cell-autonomous synaptic scaling processes

Previous work examined cell-autonomous regulation of synaptic scaling using sparse transfection of channelrhodopsins in hippocampal slices and demonstrated neurons can detect elevated activity and compensate through reducing synaptic function via AMPAR removal.[25] We wanted to test whether we can elicit this cell-autonomous regulation using our chemogenetic approach that elicits homeostatic scaling. We sparsely transfected hippocampal neurons with the mCherry-hM4D(Gi)-DREADDs on DIV 7 to create a co-culture of about 70% wild-type neurons and 30% hM4D(Gi)-expressing neurons (Figures 2K and 2L) and then we treated the entire coverslip with the DREADD ligand. This approach allowed us to circumvent altering network-wide activity and specifically manipulate individual neurons that express the Gi-DREADD. Whole-cell voltage-clamp recordings were performed on control untransfected neurons and mCherry-expressing neurons from the same coverslips on DIV15-18 following 48-h treatment with 1 μM CMPD21. Chronic activation of Gi-coupled DREADDs led to synaptic upscaling in select mCherry-expressing neurons compared to the control, evidenced by a significant increase in mEPSC amplitude with no change on mEPSC frequency (Figures 2M and 2N). We found that control neurons within the same treated coverslips did not undergo this same synaptic regulation as their neighboring neurons expressing DREADDs. Further, our observations suggest that this chemogenetic induction of scaling relies on post-synaptic regulation, whereby changes are mediated by receptor compensation and not presynaptic release (consistent with no change in event frequency). This is in line with previous work demonstrating how neurons can individually detect local perturbations and initiate cell-autonomous compensatory changes.[25–30] Our data show that DREADDs can be used to effectively study cell-autonomous effects of homeostatic synaptic plasticity by eliciting synaptic scaling in individual neurons.

hM4D(Gi)-induced upscaling is convergent on the RARα-dependent signaling pathway

Previous studies demonstrated that homeostatic synaptic scaling mechanisms driven by chronic activity blockade with TTX were mediated by an increase in AMPAR expression at the synapse.[11,31–34] Moreover, studies went on to characterize how different pharmacological manipulations gave rise to AMPAR expression through RARα signaling. Retinoic acid (RA) synthesis is upregulated to target RARα activation to upregulate AMPAR subunit synthesis in local dendrites, increasing synaptic strength while preserving relative strength between individual synapses.[1,15,35,36] Although much is known about what regulates this activity-dependent pathway of synaptic plasticity, we wanted to explore if our activity-independent pathway can recruit the RARα signaling pathway or if it is a separate pathway in itself.

In the next set of experiments, we investigated whether hM4D(Gi)-induced scaling triggers upscaling in a distinct pathway from that of traditional chronic complete activity blockade. We performed whole-cell voltage-clamp experiments on hM4D(Gi)-expressing neurons after treatment with 1 μM CMPD21 for 48 h, 5 μM AM580 (a RARα agonist)[36] for 1 h, or co-treatment of CMPD21 + AM580 to determine if scaling is augmented by RARα activation (Figure 3A). We observed no significant difference between mean mEPSC amplitudes for chronic CMPD21 + AM580 treatment compared to CMPD21 or AM580 alone, demonstrating that CMPD21 occludes the subsequent action of AM580 treatment (Figure 3B). There was no significant difference in mEPSC frequency between all treatment groups compared to DMSO control (Figure 3C). These data demonstrate that hM4D(Gi)-induced scaling is dependent on RARα activation, and the combination of the two approaches occludes further synaptic scaling.

To further answer if hM4D(Gi)-induced scaling operates through the same molecular pathway as RARα-dependent activation, we co-treated hM4D(Gi)-expressing neurons with 1 μM CMPD21 for 48 h and 5 μM citral (an inhibitor of retinoic acid synthesis)[36] for 24 h. Interestingly, we observed that citral was sufficient to block scaling induced by chronic hM4D(Gi) signaling, indicated by a return of mEPSC amplitudes down to control levels with DMSO treatment (Figures 3D and 3E). Chronic CMPD21 or co-treatment with citral did not affect mEPSC frequency across groups (Figure 3F). These results demonstrate that hM4D(Gi)-induced upscaling works via pathways targeting RA synthesis to act on the RARα-dependent pathway.

Chronically modulating cAMP triggers mechanisms of homeostatic synaptic plasticity

Since we uncovered that hM4D(Gi)-induced scaling elicits homeostatic scaling processes even with transient inhibition of action potential activity (as seen in Figure 2), we aimed to identify which molecular mediators could be initiating this signaling pathway upstream of RA synthesis. The canonical Gαi-G protein-coupled receptor (GPCR) pathway operates through the dissociated Gαi-subunit inhibiting adenylyl cyclase activity, which leads to decreased second messenger cAMP and its activity on effectors such as protein kinase A (PKA).[37,38] Therefore, we next tested if co-application of cAMP can alter the hM4D(Gi)-induced synaptic upscaling. Using hM4D(Gi)-expressing neurons, we treated cells with 1 μM CMPD21 and/or 1 μM 8-CPT-cAMP (a non-hydrolyzable cAMP analog) for 48 h. Whole-cell voltage-clamp recordings demonstrated synapses failed to undergo homeostatic scaling following co-treatment of CMPD21 + 8-CPT-cAMP, suggesting inhibition of cAMP is critical to trigger pathways necessary for scaling (Figures 4A–4C). This experiment illustrates that hM4D(Gi)-induced scaling is blocked when 8-CPT-cAMP is present, suggesting that cAMP regulation mediates this form of chemogenetic homeostatic synaptic plasticity. Thus far, our

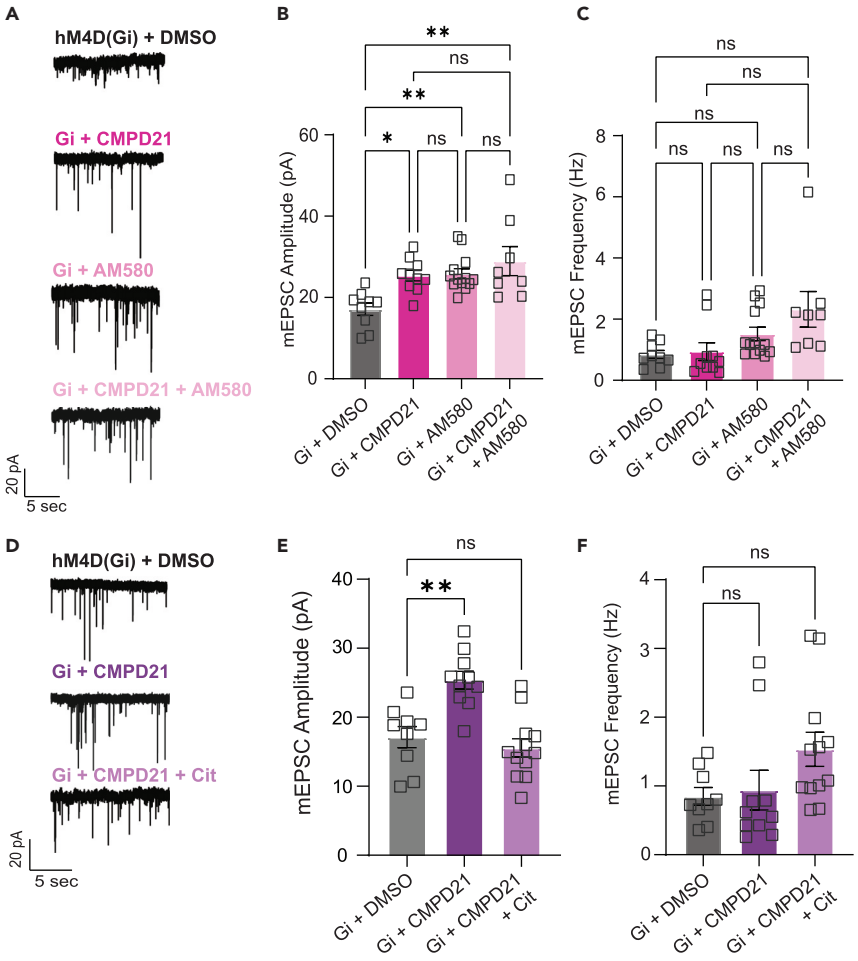

Figure 3. hM4D(Gi)-induced scaling is convergent on RARα-dependent signaling pathway

(A) Representative raw traces of mEPSCs after chronic treatment of hM4D(Gi)-expressing neurons with 48 h DMSO, 48 h 1 μM CMPD21, 1 h 5 μM AM580, or 48 h CMPD21 + 1 h AM580.

(B) Comparison of mean mEPSC amplitude (pA) following 48 h treatments with each condition (one-way ANOVA with multiple comparisons test, DMSO vs. CMPD21 $p = 0.022$; DMSO vs. AM580 $p = 0.009$; DMSO vs. CMPD21 + AM580 $p = 0.001$; CMPD21 vs. AM580 $p = 0.997$; CMPD21 vs. CMPD21 + AM580 $p = 0.588$; AM580 vs. CMPD21 + AM580 $p = 0.653$; $N = 2–3$, $n = 8–13$ per group). (C) Comparison of mean mEPSC frequency (Hz) following treatments with each condition (one-way ANOVA with multiple comparisons test, DMSO vs. CMPD21 $p = 0.999$; DMSO vs. AM580 $p = 0.092$; DMSO vs. CMPD21 + AM580 $p = 0.179$; CMPD21 vs. AM580 $p = 0.529$; CMPD21 vs. CMPD21 + AM580 $p = 0.271$; AM580 vs. CMPD21 + AM580 $p = 0.730$; $N = 2–3$, $n = 8–13$ per group). (D) Representative raw traces of mEPSCs after chronic treatments of hM4D(Gi)-expressing neurons with 48 h DMSO, 48 h 1 μM CMPD21, 24 h 5 μM citral (Cit), 48 h CMPD21 + 24 h Cit.

(E) Comparison of mean mEPSC amplitude (pA) following treatments with each condition (one-way ANOVA followed by Dunnett's multiple comparisons test DMSO vs. CMPD21 $p = 0.001$; DMSO vs. CMPD21 + Cit $p = 0.693$, $N = 1–3$, $n = 11–13$). (F) Comparison of mean mEPSC frequency (Hz) following treatments with each condition (one-way ANOVA followed by Dunnett's multiple comparisons test DMSO vs. CMPD21 $p = 0.947$; DMSO vs. CMPD21 + Cit $p = 0.051$; $N = 1–3$, $n = 11–13$). Data are represented as mean ± SEM. Significant symbols used in figures are defined as such: $*p < 0.05$; $**p < 0.01$; $***p < 0.001$; n.s.

results indicate that hM4D(Gi)-induced scaling is sufficient to activate the RARα mediated by RA synthesis and propose cAMP downregulation as an upstream mechanism for hM4D(Gi)-dependent synaptic upscaling.

To examine if the hM4D(Gi)-signaling cascade is operating through cAMP to initiate this homeostatic synaptic scaling mechanism, we sought to reproduce this effect through chronically modulating cAMP signaling in wild-type neurons.[37] In wild-type cultures, we treated neurons with 10 μM cAMPS-RP (a cAMP antagonist) for 48 h and observed a significant increase in mEPSC amplitudes following chronic blockade of cAMP. This scaling effect was sensitive to blockade of RA synthesis since co-application with the RA synthesis blocker, citral for 24 h, suppressed the synaptic scaling (Figures 4D–4F). It is important to note that we also tested acute application of cAMPS-RP (both acute recordings with cAMPS-RP in bath, or following 1 h treatment) and found it did not impact mEPSC amplitudes (control, 14.92 ± 2.33 pA; bath-cAMPS-RP, 13.41 ± 0.812 pA; 1 h cAMPS-RP, 13.06 ± 0.998 pA, $N=2$, $n = 7–8$, $p > 0.35$ for all, one-way ANOVA with Dunnett's test). To further dissect if the Gi-signaling cascade in wild-type neurons is dependent on disrupting cAMP action, we inhibited

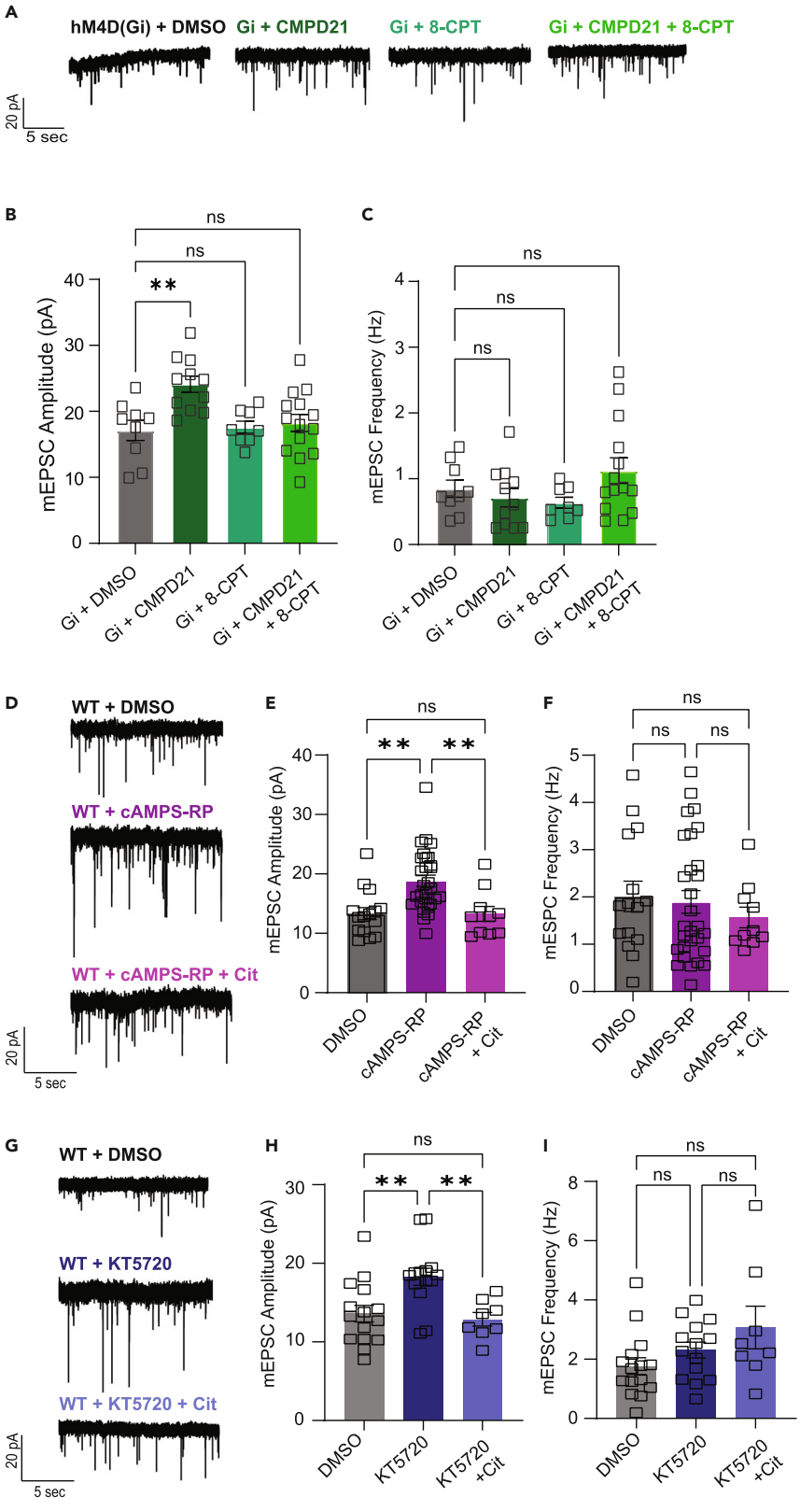
A
hM4D(Gi) + DMSO
Gi + CMPD21
Gi + 8-CPT
Gi + CMPD21 + 8-CPT
20 pA
5 sec
B
mEPSC Amplitude (pA)
ns
ns
**
Gi + DMSO
Gi + CMPD21
Gi + 8-CPT
Gi + CMPD21 + 8-CPT
C
mEPSC Frequency (Hz)
ns
ns
ns
D
WT + DMSO
WT + cAMPS-RP
WT + cAMPS-RP + Cit
20 pA
5 sec
E
mEPSC Amplitude (pA)
ns
**
**
DMSO
cAMPS-RP
cAMPS-RP + Cit
F
mESPC Frequency (Hz)
ns
ns
ns
DMSO
cAMPS-RP
cAMPS-RP + Cit
G
WT + DMSO
WT + KT5720
WT + KT5720 + Cit
20 pA
5 sec
H
mEPSC Amplitude (pA)
ns
**
**
DMSO
KT5720
KT5720 +Cit
I
mEPSC Frequency (Hz)
ns
ns
ns
DMSO
KT5720
KT5720 +Cit

Figure 4. Chronically modulating cAMP triggers mechanisms of homeostatic synaptic plasticity

(A) Representative raw traces of mEPSCs after chronic treatment of hM4D(Gi)-expressing neurons with 48 h DMSO, 48 h 1 μM CMPD21, 48 h 1 μM 8-CPT, and 48 h CMPD21 + 8-CPT (B) Comparison of mean mEPSC amplitude (pA) following treatments with each condition (one-way ANOVA with Dunnett's multiple comparisons test DMSO vs. CMPD21 $p = 0.007$; DMSO vs. 8-CPT $p = 0.990$; DMSO vs. CMPD21 + 8-CPT $p = 0.922$, $N = 2$, $n = 8–14$ per group). (C) Comparison of mean mEPSC frequency (Hz) following treatments with each condition (one-way ANOVA followed by Dunnett's multiple comparison DMSO vs. CMPD21 $p = 0.854$; DMSO vs. 8-CPT $p = 0.458$; DMSO vs. CMPD21 + 8-CPT $p = 0.569$; $N = 2$, $n = 8–14$ per group). (D) Representative raw traces of mEPSCs after treatment of WT cultures with 48 h DMSO or cAMPS-RP.

(E) Comparison of mEPSC amplitude (pA) after 48 h treatment of DMSO or 10 μM cAMPS-RP in WT cultures (one-way ANOVA followed by Tukey's multiple comparison DMSO vs. cAMPS-RP $p = 0.001$; DMSO vs. cAMPS-RP + Cit $p = 0.999$; cAMPS-RP vs. cAMPS-RP + Cit $p = 0.005$, $N = 2–4$, $n = 11–31$). (F) Comparison of mEPSC frequency (Hz) after 48 h treatment of DMSO or 10 μM cAMPS-RP (one-way ANOVA followed by Tukey's multiple comparison DMSO vs. cAMPS-RP $p = 0.883$; DMSO vs. cAMPS-RP + Cit $p = 0.637$; cAMPS-RP vs. cAMPS-RP + Cit $p = 0.821$; $N = 2–4$, $n = 11–31$). (G) Representative raw traces of mEPSCs after treatment of WT cultures with DMSO or 1 μM KT5720. (H) Comparison of mEPSC amplitude (pA) after 48 h treatment of DMSO or KT5720 (one-way ANOVA followed by Tukey's multiple comparison DMSO vs. KT5720 $p = 0.005$; DMSO vs. KT5720 + Cit $p = 0.905$; KT5720 vs. KT5720 + Cit $p = 0.008$; $N = 2$, $n = 8–15$).

(I) Comparison of mEPSC frequency (Hz) after 48 h treatment of DMSO or 1 μM KT5720 (one-way ANOVA followed by Dunnett's multiple comparison DMSO vs. KT5720 $p = 0.513$; DMSO vs. KT5720 + Cit $p = 0.076$; KT5720 vs. KT5720 + Cit $p = 0.407$; $N = 2$, $n = 8–15$). Data are represented as mean ± SEM. Significant symbols used in figures are defined as such: $*p < 0.05$; $**p < 0.01$; $***p < 0.001$; n.s.

subsequent target proteins to verify if it effectively elicits this synaptic scaling mechanism. We treated neurons with 1 μM KT5720 (PKA inhibitor) for 48 h and a similar pattern was observed with a significant increase in mEPSC amplitude following chronic treatment, with synaptic upscaling blocked by co-application of citral (Figures 4G–4I). Taken together, these data show that synaptic scaling can be effectively triggered by chronic modulation of Gi-signaling proteins, initiated by a decrease in cAMP action on PKA. This set of experiments illustrates that chronically blocking cAMP function induces synaptic scaling dependent on RARα signaling, suggesting RA synthesis mediates this pathway. Overall, our data provide evidence that directly regulating cAMP levels presents a direct activity-independent mechanism of homeostatic synaptic scaling at excitatory synapses.

Homeostatic upscaling via cAMP is regulated by CP-AMPARs

Several studies that observed homeostatic synaptic plasticity using pharmacological methods reported that inhibition of excitatory synaptic transmission in cultured neurons upregulated GluA2-lacking AMPARs, also called CP-AMPARs, at the synapse.[31–33] The recruitment of CP-AMPARs has been shown to be regulated by GluA1 synthesis in dendrites, underlying the translation of necessary subunits of GluA2-lacking AMPARs.[15,36,39,40] Since we found that cAMP modulation can trigger homeostatic synaptic plasticity, we wanted to investigate if this was driven by CP-AMPAR insertion using the CP-AMPAR antagonist, 1-naphthylacetyl spermine (NASPM) trihydrochloride. In wild-type cultures, we treated neurons with 10 μM cAMPS-RP for 48 h to elicit upscaling and recorded from the same neuron continuously with a baseline followed by 50 μM NASPM trihydrochloride perfusion. We reproduced upscaling seen by a significant increase in mEPSC amplitudes (Figures 5A and 5B), with NASPM perfusion exhibiting a significant decrease in mEPSC amplitude immediately following acute wash of the CP-AMPAR antagonist. No significant difference was observed following acute perfusion of NASPM on DMSO-treated cultures, or in mEPSC frequency across the groups (Figure 5C).

After elucidating the activity-independent homeostatic upscaling via Gi-DREADD manipulation, we aimed to confirm the effect of NASPM in Gi-expressing cultures. In lentiviral Gi-DREADD-expressing cultures, we treated neurons with 1 μM CMPD21 for 48 h and repeated the same procedure of continuous recordings with a baseline followed by 50 μM NASPM trihydrochloride perfusion. Indeed, synaptic upscaling was observed following chronic CMPD21 treatment, with a rapid decrease in mEPSC amplitude upon acute NASPM perfusion (Figures 5D–5F). This set of acute perfusion experiments demonstrates that homeostatic upscaling induced by cAMP-mediated signaling relies on insertion of CP-AMPARs at the synapse.

DISCUSSION

Studies on homeostatic synaptic plasticity have largely focused on regulation of neuronal activity or synaptic transmission primarily using specific activity blockers. Here, we used inhibitory DREADDs to probe molecular mediators that regulate homeostatic plasticity mechanisms, a strategy that has been similarly used *in vivo* to study homeostatic plasticity during development.[5] We validated the efficacy of DREADD manipulation using agonist Compound 21, which we used to chronically activate hM4D(Gi) signaling. We discovered that action potential activity is mildly suppressed but later adapts to the hM4D(Gi)-induced low-activity environment. We found that chronic activation of the hM4D(Gi)-DREADDs induced mechanisms of homeostatic synaptic plasticity that converges on the RARα-dependent signaling pathway. We demonstrated this RARα pathway can be effectively triggered by blocking the function of Gαi-signaling proteins, cAMP and PKA. Our findings demonstrate that neurons can autonomously detect downregulation of these signaling proteins, triggering mechanisms of homeostatic synaptic plasticity. Furthermore, we show that this upscaling relies on insertion of CP-AMPARs at the synapse.

Through a series of experiments, we discovered that hM4D(Gi)-induced synaptic upscaling pathway converges onto the well-characterized RARα-dependent synaptic signaling.[1,18] RA and its receptor target, the RARα, have been established as a critical mediator for homeostatic synaptic plasticity for enhancing excitatory synaptic strength.[15,39] Silencing neuronal activity with pharmacological drugs triggers the production of RA which binds to RARα receptors localized to synapses, leading to translation of CP-AMPARs, underlying upscaling.[36] However,

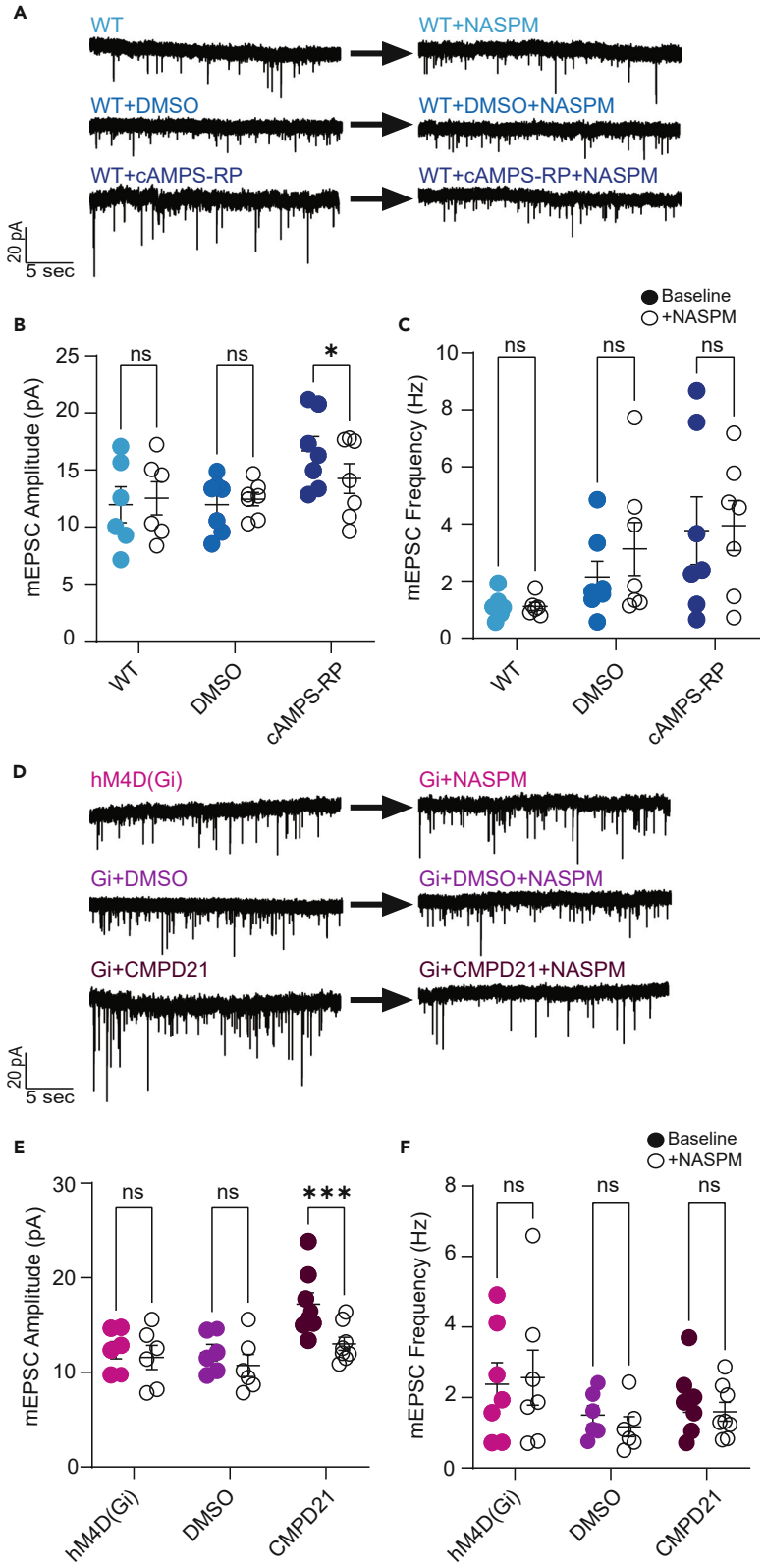
A
WT
WT+NASPM
WT+DMSO
WT+DMSO+NASPM
WT+cAMPS-RP
WT+cAMPS-RP+NASPM
20 pA
5 sec
B
mEPSC Amplitude (pA)
ns
ns
*
WT
DMSO
cAMPS-RP
C
Baseline
+NASPM
mEPSC Frequency (Hz)
ns
ns
ns
WT
DMSO
cAMPS-RP
D
hM4D(Gi)
Gi+NASPM
Gi+DMSO
Gi+DMSO+NASPM
Gi+CMPD21
Gi+CMPD21+NASPM
20 pA
5 sec
E
mEPSC Amplitude (pA)
ns
ns
***
hM4D(Gi)
DMSO
CMPD21
F
Baseline
+NASPM
mEPSC Frequency (Hz)
ns
ns
ns
hM4D(Gi)
DMSO
CMPD21

Figure 5. Homeostatic upscaling via cAMP is regulated by CP-AMPARs

(A) Representative raw traces of wild-type mEPSCs before (left) and after (right) acute perfusion of 50 μM NASPM trihydrochloride on cultures that underwent no treatment, 48 h DMSO, or 48 h 10 μM cAMPS-RP.

(B) Comparison of mEPSC amplitude (pA) after no treatment, DMSO, or 10 μM cAMPS-RP (two-way ANOVA with Sidak's multiple comparisons test; WT vs. WT + NASPM $p = 0.910$; WT-DMSO vs. WT-DMSO + NASPM $p = 0.932$; WT-cAMPS-RP vs. WT-cAMPS-RP + NASPM $p = 0.035$; $N = 4$, $n = 6–7$ per group). (C) Comparison of mEPSC frequency (Hz) after no treatment, DMSO, or cAMPS-RP (two-way ANOVA with Sidak's multiple comparisons test; WT vs. WT + NASPM $p > 0.999$; WT-DMSO vs. WT-DMSO + NASPM $p = 0.376$; WT-cAMPS-RP vs. WT-cAMPS-RP + NASPM $p = 0.990$; $N = 4$, $n = 6–7$ per group). (D) Representative raw traces of Gi-DREADD mEPSCs before (left) and after (right) acute perfusion of 50 μM NASPM trihydrochloride on cultures that underwent no treatment, 48 h DMSO, or 48 h 1 μM CMPD21.

(E) Comparison of mEPSC amplitude (pA) after no treatment, 48 h treatment of DMSO, or 48 h 1 μM CMPD21 (two-way ANOVA with Sidak's multiple comparisons test; Gi vs. Gi + NASPM $p = 0.834$; Gi-DMSO vs. Gi-DMSO + NASPM $p = 0.363$; Gi-CMPD21 vs. Gi-CMPD21 + NASPM $p = 0.0004$; $N = 4$, $n = 6–7$ per group). (F) Comparison of mEPSC frequency (Hz) after no treatment, 48 h treatment of DMSO, or 48 h 1 μM CMPD21 (two-way ANOVA with Sidak's multiple comparisons test; Gi vs. Gi + NASPM $p = 0.893$; Gi-DMSO vs. Gi-DMSO + NASPM $p = 0.697$; Gi-CMPD21 vs. Gi-CMPD21 + NASPM $p = 0.615$; $N = 4$, $n = 6–7$ per group). Data are represented as mean ± SEM. Significant symbols used in figures are defined as such: $*p < 0.05$; $**p < 0.01$; $***p < 0.001$; n.s.

induction of this pathway via other upstream molecular signals has not been identified. Our experiments showed that direct RARα activation occludes further hM4D(Gi)-induced synaptic scaling, illustrating the Gi-induced and TTX-induced signaling pathway converge on RARα-dependent mechanisms. Here, we observe that longer durations of activity blockade with TTX alone may be similarly acting on the RARα-dependent pathway for upscaling, which was not thought to be associated before this study. In earlier studies, the process of using TTX alone to block activity shows increased mEPSC amplitude as a linear progression with treatment time (when comparing 26 to 48 h), suggesting that continual silencing may engage protein synthesis through RA signaling in the case of chronic TTX-mediated synaptic scaling.[11,34] Studying cellular mechanisms using chronic blockade of activity with TTX was not the focus of this study; however, it would be interesting for future studies to test whether RA synthesis and CP-AMPAR insertion is directly observed using various durations of TTX treatment.

Further, we showed that inhibiting RA synthesis blocked the induction of homeostatic scaling triggered by chronic hM4D(Gi) signaling, suggesting RA synthesis is necessary for this pathway. These experiments demonstrate that hM4D(Gi) signaling can activate the RARα-dependent signaling pathway, inducing homeostatic plasticity mechanisms. This result expands our mechanistic understanding of traditional GPCR signaling since we demonstrate for the first time how dynamic Gαi-signaling can activate RA synthesis.

Further, we investigated how modulation of cAMP orchestrates this Gi-signaling cascade that targets the RARα-dependent signaling pathway. As Gαi-GPCR functions to inhibit adenylyl cyclase activity, which decreases cAMP and its activity on downstream effectors, we targeted steps in this cascade.[38] In wild-type neurons, we showed that chronically blocking cAMP activity is sufficient to trigger classic homeostatic synaptic upscaling. Concomitantly, we showed that blocking the downstream second messenger target—PKA—also triggers synaptic upscaling associated with homeostatic synaptic plasticity. Strikingly, scaling was prevented in both conditions by blocking RA synthesis, consistent with RARα-dependent signaling requiring RA production. Overall, we demonstrated how manipulation of cAMP and PKA in the Gαi-signaling cascade can elicit mechanisms of homeostatic synaptic scaling across the neuronal network, which converge upon RARα-dependent signaling.

Finally, we dissected how upscaling triggered by cAMP modulation is regulated by insertion of CP-AMPARs at the synapse. Earlier work has shown that homeostatic synaptic upscaling driven by the RARα-dependent signaling pathway activates synthesis of subunits for CP-AMPAR.[15,40] We first tested this premise using wild-type neurons where we demonstrated that chronically manipulating cAMP to induce synaptic upscaling can be rapidly blocked by perfusing a CP-AMPAR antagonist, NASPM trihydrochloride. We successfully reproduced this same effect using the Gi-DREADD model to induce synaptic upscaling, which also showed a decrease in post-synaptic response amplitudes within minutes of NASPM perfusion. This set of experiments illustrates how the synaptic upscaling elicited by cAMP modulation reliably activates the RARα-dependent signaling pathway to regulate CP-AMPAR synthesis for modifying the synapse in homeostatic synaptic processes.

By recapitulating an environment that closely mimics a system with ongoing sustained activity, our data uncover a signaling pathway that elicits scaling irrespective of network activity. This finding expands the repertoire of tools for regulation of synaptic scaling without drastic manipulation of activity, such as the role of spontaneous inhibitory neurotransmission in brain-derived neurotrophic factor regulation which functions to modulate synaptic strength.[41,42] Exploiting approaches that bypass activity regulation will further shed light on how neurons can re-adjust or scale synaptic signaling patterns within functioning networks. Our results indicate that in the presence of activity, chronic modulation of Gαi-GPCR-mediated reduction in cAMP signaling converges on the RARα-dependent pathway to induce homeostatic synaptic plasticity. No reported association between cAMP regulations affecting RA synthesis has been documented in the literature, thus future research directions aim to identify mediators of this dynamic crosstalk. More recently, tools were recently developed to enable suppression of local cAMP in subcellular compartments for understanding synapse assembly.[43] This candidate tool enables future studies to explore the functional consequences of locally modulating cAMP in driving homeostatic synaptic plasticity, with the hope of identify subsequent targets.

When taken together with recent studies, these results highlight a substantial degeneracy in mechanisms that elicit homeostatic synaptic scaling. Although initial work emphasized activity[11] as a major determinant of homeostatic regulation of synaptic strength, activity-independent mechanisms appear to play equally important roles.[18,19,29,39,44–46] Synapses operate under a constant barrage of signals that include G protein-dependent second messenger cascades, Ca^{2+} signaling, as well as fast ionotropic signaling, in addition to the arrival of action

potentials. Therefore, synaptic homeostasis must be maintained in the midst of diverse and sometimes conflicting signals. The mechanisms we uncovered here suggest that synapses have the flexibility to adapt and establish their set point appropriately, even amid continuous cellular signals and activity.

Limitations of the study

This study has uncovered that prolonged inhibition of cAMP via the Gαi-GPCR signaling cascade leads to the induction of homeostatic synaptic plasticity. Moreover, this mechanism converges on the RARα-dependent pathway to activate the synthesis of CP-AMPARs. Though we demonstrate how direct modulation of molecular mediators in the Gαi-GPCR activates homeostatic processes, further investigation is needed to elucidate the direct downstream effectors that activate the RARα signaling pathway. This study has raised new questions about how neurons detect activity-independent signals for triggering homeostatic mechanisms. A limitation of this study is that pharmacological approaches to alter cAMP signaling affect cAMP globally within a cell. Therefore, future studies need to address spatially restricting cAMP suppression to enhance our understanding of how neurons initiate homeostatic processes via local perturbations. Since we show that this activity-independent mechanism of homeostatic synaptic plasticity relies on RARα activation for CP-AMPAR insertion, it may be important to study the timescale of this RARα pathway activation and AMPAR composition at the synapse. This present study lays ground by demonstrating that cAMP modulation alone can induce homeostatic synaptic plasticity amid ongoing activity.

STAR★METHODS

Detailed methods are provided in the online version of this paper and include the following:

- KEY RESOURCES TABLE
- RESOURCE AVAILABILITY
  - Lead contact
  - Materials availability
  - Data and code availability
- EXPERIMENTAL MODEL AND STUDY PARTICIPANT DETAILS
  - Animals
  - Primary hippocampal culture preparation
- METHOD DETAILS
  - Sparse neuron transfection
  - Immunocytochemistry and imaging
  - Drug treatment
  - Electrophysiology
- QUANTIFICATION AND STATISTICAL ANALYSIS

SUPPLEMENTAL INFORMATION

Supplemental information can be found online at https://doi.org/10.1016/j.isci.2024.110176.

ACKNOWLEDGMENTS

We would like to thank Brent Trauterman for his assistance in generating the constructs and Dr. Kanzo Suzuki for his guidance in experimental techniques. We also thank Natalie Guzikowski, Clara McCarthy, and Christine Saunders for their insightful comments on the manuscript. This work was supported by the National Institute of Mental Health (grant R01NS134128 to E.T.K. and T32 MH064913 to E.D.B.). Figure 1A was created with BioRender.com.

AUTHOR CONTRIBUTIONS

E.D.B. and E.T.K. planned the study. E.D.B. executed experiments for the study and analyzed the data. E.D.B. and E.T.K. wrote and edited the manuscript.

DECLARATION OF INTERESTS

The authors declare no competing interests.

Received: January 22, 2024
Revised: April 11, 2024
Accepted: May 31, 2024
Published: June 5, 2024

REFERENCES

1. Zhong, L.R., Chen, X., Park, E., Südhof, T.C., and Chen, L. (2018). Retinoic acid receptor RARα-dependent synaptic signaling mediates homeostatic synaptic plasticity at the inhibitory synapses of mouse visual cortex. J. Neurosci. *38*, 10454–10466. https://doi.org/10.1523/JNEUROSCI.1133-18.2018.
2. Ljaschenko, D., Ehmann, N., and Kittel, R.J. (2013). Hebbian Plasticity Guides Maturation of Glutamate Receptor Fields InVivo. Cell Rep. *3*, 1407–1413. https://doi.org/10.1016/j.celrep.2013.04.003.
3. Turrigiano, G.G. (2008). The self-tuning neuron: synaptic scaling of excitatory synapses. Cell *135*, 422–435. https://doi.org/10.1016/J.CELL.2008.10.008.
4. Kavalali, E.T., and Monteggia, L.M. (2020). Targeting Homeostatic Synaptic Plasticity for Treatment of Mood Disorders. Neuron *106*, 715–726. https://doi.org/10.1016/j.neuron.2020.05.015.
5. Wen, W., and Turrigiano, G.G. (2021). Developmental Regulation of Homeostatic Plasticity in Mouse Primary Visual Cortex. J. Neurosci. *41*, 9891–9905. https://doi.org/10.1523/JNEUROSCI.1200-21.2021.
6. Thompson, K.J., Khajehali, E., Bradley, S.J., Navarrete, J.S., Huang, X.P., Slocum, S., Jin, J., Liu, J., Xiong, Y., Olsen, R.H.J., et al. (2018). DREADD Agonist 21 is an effective agonist for muscarinic-based DREADDs *in vitro* and *in vivo*. ACS Pharmacol. Transl. Sci. *1*, 61–72. https://doi.org/10.1021/ACSPTSCI.8B00012.
7. Xin, J., Shan, W., Li, J., Yu, H., and Zuo, Z. (2022). Activation of the Lateral Habenula-Ventral Tegmental Area Neural Circuit Contributes to Postoperative Cognitive Dysfunction in Mice. Adv. Sci. *9*, e2202228. https://doi.org/10.1002/advs.202202228.
8. Liou, C.-W., Cheng, S.-J., Yao, T.-H., Lai, T.-T., Tsai, Y.-H., Chien, C.-W., Kuo, Y.-L., Chou, S.-H., Hsu, C.-C., and Wu, W.-L. (2023). Microbial metabolites regulate social novelty via CaMKII neurons in the BNST. Brain Behav. Immun. *113*, 104–123. https://doi.org/10.1016/j.bbi.2023.06.029.
9. Institoris, A., Vandal, M., Peringod, G., Catalano, C., Tran, C.H., Yu, X., Visser, F., Breiteneder, C., Molina, L., Khakh, B.S., et al. (2022). Astrocytes amplify neurovascular coupling to sustained activation of neocortex in awake mice. Nat. Commun. *13*, 7872. https://doi.org/10.1038/s41467-022-35383-2.
10. Turrigiano, G. (2012). Homeostatic synaptic plasticity: Local and global mechanisms for stabilizing neuronal function. Cold Spring Harbor Perspect. Biol. *4*, a005736. https://doi.org/10.1101/cshperspect.a005736.
11. Turrigiano, G.G., Leslie, K.R., Desai, N.S., Rutherford, L.C., and Nelson, S.B. (1998). Activity-dependent scaling of quantal amplitude in neocortical neurons. Nature *391*, 892–896. https://doi.org/10.1038/36103.
12. Venkatesan, S., Subramaniam, S., Rajeev, P., Chopra, Y., Jose, M., and Nair, D. (2020). Differential Scaling of Synaptic Molecules within Functional Zones of an Excitatory Synapse during Homeostatic Plasticity. eNeuro *7*, 1–16. https://doi.org/10.1523/ENEURO.0407-19.2020.
13. Stellwagen, D., and Malenka, R.C. (2006). Synaptic scaling mediated by glial TNF-α. Nature *440*, 1054–1059. https://doi.org/10.1038/nature04671.
14. Wu, C.H., Ramos, R., Katz, D.B., and Turrigiano, G.G. (2021). Homeostatic synaptic scaling establishes the specificity of an associative memory. Curr. Biol. *31*, 2274–2285.e5. https://doi.org/10.1016/j.cub.2021.03.024.
15. Maghsoodi, B., Poon, M.M., Nam, C.I., Aoto, J., Ting, P., and Chen, L. (2008). Retinoic acid regulates RARalpha-mediated control of translation in dendritic RNA granules during homeostatic synaptic plasticity. Proc. Natl. Acad. Sci. USA *105*, 16015–16020. https://doi.org/10.1073/pnas.0804801105.
16. Ranson, A., Cheetham, C.E.J., Fox, K., and Sengpiel, F. (2012). Homeostatic plasticity mechanisms are required for juvenile, but not adult, ocular dominance plasticity. Proc. Natl. Acad. Sci. USA *109*, 1311–1316. https://doi.org/10.1073/PNAS.1112204109.
17. Krahe, T.E., and Guido, W. (2011). Homeostatic plasticity in the visual thalamus by monocular deprivation. J. Neurosci. *31*, 6842–6849. https://doi.org/10.1523/JNEUROSCI.1173-11.2011.
18. Suzuki, K., Kim, J.W., Nosyreva, E., Kavalali, E.T., and Monteggia, L.M. (2021). Convergence of distinct signaling pathways on synaptic scaling to trigger rapid antidepressant action. Cell Rep. *37*, 109918. https://doi.org/10.1016/J.CELREP.2021.109918.
19. Reese, A.L., and Kavalali, E.T. (2015). Spontaneous neurotransmission signals through store-driven Ca2+ transients to maintain synaptic homeostasis. Elife *4*, e09262. https://doi.org/10.7554/ELIFE.09262.001.
20. Ibata, K., Sun, Q., and Turrigiano, G.G. (2008). Rapid Synaptic Scaling Induced by Changes in Postsynaptic Firing. Neuron *57*, 819–826. https://doi.org/10.1016/j.neuron.2008.02.031.
21. Keck, T., Keller, G.B., Jacobsen, R.I., Eysel, U.T., Bonhoeffer, T., and Hübener, M. (2013). Synaptic scaling and homeostatic plasticity in the mouse visual cortex *in vivo*. Neuron *80*, 327–334. https://doi.org/10.1016/j.neuron.2013.08.018.
22. Wang, X., Wang, Q., Yang, S., Bucan, M., Rich, M.M., and Engisch, K.L. (2011). Impaired activity-dependent plasticity of quantal amplitude at the neuromuscular junction of Rab3A Deletion and Rab3A earlybird mutant mice. J. Neurosci. *31*, 3580–3588. https://doi.org/10.1523/JNEUROSCI.5278-10.2011.
23. Tan, H.L., Queenan, B.N., and Huganir, R.L. (2015). GRIP1 is required for homeostatic regulation of AMPAR trafficking. Proc. Natl. Acad. Sci. USA *112*, 10026–10031. https://doi.org/10.1073/pnas.1512786112.
24. Shen, N., Wang, B., Soto, F., and Kerschensteiner, D. (2020). Homeostatic Plasticity Shapes the Retinal Response to Photoreceptor Degeneration. Curr. Biol. *30*, 1916–1926.e3. https://doi.org/10.1016/j.cub.2020.03.033.
25. Goold, C.P., and Nicoll, R.A. (2010). Single-Cell Optogenetic Excitation Drives Homeostatic Synaptic Depression. Neuron *68*, 512–528. https://doi.org/10.1016/J.NEURON.2010.09.020.
26. Khajeh, R., Fumarola, F., and Abbott, L.F. (2022). Sparse balance: Excitatory-inhibitory networks with small bias currents and broadly distributed synaptic weights. PLoS Comput. Biol. *18*, e1008836. https://doi.org/10.1371/journal.pcbi.1008836.
27. Desai, N.S., Rutherford, L.C., and Turrigiano, G.G. (1999). Plasticity in the intrinsic excitability of cortical pyramidal neurons. Nat. Neurosci. *2*, 515–520. https://doi.org/10.1038/9165.
28. Marder, E., and Prinz, A.A. (2002). Modeling stability in neuron and network function: The role of activity in homeostasis. Bioessays *24*, 1145–1154. https://doi.org/10.1002/BIES.10185.
29. Nosyreva, E., Szabla, K., Autry, A.E., Ryazanov, A.G., Monteggia, L.M., and Kavalali, E.T. (2013). Acute suppression of spontaneous neurotransmission drives synaptic potentiation. J. Neurosci. *33*, 6990–7002. https://doi.org/10.1523/JNEUROSCI.4998-12.2013.
30. Blackman, M.P., Djukic, B., Nelson, S.B., and Turrigiano, G.G. (2012). A critical and cell-autonomous role for MeCP2 in synaptic scaling up. J. Neurosci. *32*, 13529–13536. https://doi.org/10.1523/JNEUROSCI.3077-12.2012.
31. Lee, H.K. (2012). Ca 2+-permeable AMPA receptors in homeostatic synaptic plasticity. Front. Mol. Neurosci. *5*, 15671. https://doi.org/10.3389/FNMOL.2012.00017.
32. O'Brien, R.J., Kamboj, S., Ehlers, M.D., Rosen, K.R., Fischbach, G.D., and Huganir, R.L. (1998). Activity-Dependent Modulation of Synaptic AMPA Receptor Accumulation. Neuron *21*, 1067–1078. https://doi.org/10.1016/S0896-6273(00)80624-8.
33. Hou, Q., Zhang, D., Jarzylo, L., Huganir, R.L., and Man, H.Y. (2008). Homeostatic regulation of AMPA receptor expression at single hippocampal synapses. Proc. Natl. Acad. Sci. USA *105*, 775–780. https://doi.org/10.1073/PNAS.0706447105.
34. Han, E.B., and Stevens, C.F. (2009). Development regulates a switch between postand presynaptic strengthening in response to activity deprivation. Proc. Natl. Acad. Sci. USA *106*, 10817–10822. https://doi.org/10.1073/PNAS.0903603106.
35. Thapliyal, S., Arendt, K.L., Lau, A.G., and Chen, L. (2022). Retinoic acid-gated BDNF synthesis in neuronal dendrites drives presynaptic homeostatic plasticity. Elife *11*, e79863. https://doi.org/10.7554/ELIFE.79863.
36. Aoto, J., Nam, C.I., Poon, M.M., Ting, P., and Chen, L. (2008). Synaptic Signaling by All-Trans Retinoic Acid in Homeostatic Synaptic Plasticity. Neuron *60*, 308–320. https://doi.org/10.1016/j.neuron.2008.08.012.
37. Tilley, D.G. (2011). G protein-dependent and G protein-independent signaling pathways and their impact on cardiac function. Circ. Res. *109*, 217–230. https://doi.org/10.1161/CIRCRESAHA.110.231225.
38. Batty, N.J., Fenrich, K.K., and Fouad, K. (2017). The role of cAMP and its downstream targets in neurite growth in the adult nervous system. Neurosci. Lett. *652*, 56–63. https://doi.org/10.1016/j.neulet.2016.12.033.
39. Sutton, M.A., Ito, H.T., Cressy, P., Kempf, C., Woo, J.C., and Schuman, E.M. (2006). Miniature Neurotransmission Stabilizes Synaptic Function via Tonic Suppression of Local Dendritic Protein Synthesis. Cell *125*, 785–799. https://doi.org/10.1016/j.cell.2006.03.040.
40. Poon, M.M., and Chen, L. (2008). Retinoic acid-gated sequence-specific translational control by RARalpha. Proc. Natl. Acad. Sci. USA *105*, 20303–20308. https://doi.org/10.1073/PNAS.0807740105.

41. Horvath, P.M., Chanaday, N.L., Alten, B., Kavalali, E.T., and Monteggia, L.M. (2021). A subthreshold synaptic mechanism regulating BDNF expression and resting synaptic strength. Cell Rep. *36*, 109467. https://doi.org/10.1016/J.CELREP.2021.109467.
42. Guzikowski, N.J., and Kavalali, E.T. (2022). Nano-organization of spontaneous GABAergic transmission directs its autonomous function in neuronal signaling. Cell Rep. *40*, 111172. https://doi.org/10.1016/J.CELREP.2022.111172.
43. Sando, R., Ho, M.L., Liu, X., and Südhof, T.C. (2022). Engineered synaptic tools reveal localized cAMP signaling in synapse assembly. J. Cell Biol. *221*, e202109111. https://doi.org/10.1083/JCB.202109111.
44. Fong, M.F., Newman, J.P., Potter, S.M., and Wenner, P. (2015). Upward synaptic scaling is dependent on neurotransmission rather than spiking. Nat. Commun. *6*, 6339. https://doi.org/10.1038/ncomms7339.
45. Crawford, D.C., Ramirez, D.M.O., Trauterman, B., Monteggia, L.M., and Kavalali, E.T. (2017). Selective molecular impairment of spontaneous neurotransmission modulates synaptic efficacy. Nat. Commun. *8*, 14436. https://doi.org/10.1038/NCOMMS14436.
46. Styr, B., Gonen, N., Zarhin, D., Ruggiero, A., Atsmon, R., Gazit, N., Braun, G., Frere, S., Vertkin, I., Shapira, I., et al. (2019). Mitochondrial Regulation of the Hippocampal Firing Rate Set Point and Seizure Susceptibility. Neuron *102*, 1009–1024.e8. https://doi.org/10.1016/j.neuron.2019.03.045.
47. Schindelin, J., Arganda-Carreras, I., Frise, E., Kaynig, V., Longair, M., Pietzsch, T., Preibisch, S., Rueden, C., Saalfeld, S., Schmid, B., et al. (2012). Fiji: an open-source platform for biological-image analysis. Nat. Methods *9*, 676–682. https://doi.org/10.1038/nmeth.2019.
48. Kavalali, E.T., Klingauf, J., and Tsien, R.W. (1999). Activity-dependent regulation of synaptic clustering in a hippocampal culture system. Proc. Natl. Acad. Sci. USA *96*, 12893–12900. https://doi.org/10.1073/pnas.96.22.12893.
49. Sando, R., Jiang, X., and Südhof, T.C. (2019). Latrophilin GPCRs direct synapse specificity by coincident binding of FLRTs and teneurins. Science *363*, eaav7969. https://doi.org/10.1126/science.aav7969.

STAR★METHODS

KEY RESOURCES TABLE

REAGENT or RESOURCE	SOURCE	IDENTIFIER
Antibodies		
Rat monoclonal anti-mCherry	Thermo Fisher Scientific	Cat#M11217; RRID: AB_2536611
Guinea pig polyclonal anti-MAP2	Synaptic Systems	Cat#188004
Goat anti-guinea pig IgG (H + L) Highly Cross Adsorbed Secondary Antibody, Alexa Fluor 488	Thermo Fisher Scientific	Cat# A11073; RRID: AB_2534117
Goat anti-rabbit, Highly Cross Adsorbed Secondary Antibody, Alexa Fluor 594	Thermo Fisher Scientific	Cat#A11037; RRID: AB_2534095
Chemicals, peptides, and recombinant proteins		
AM580	Cayman	Cat#14261
DMSO	Sigma	Cat#D2650
Paraformaldehyde	Sigma	Cat#P6148
Normal goat serum	Vector Laboratories	Cat#S-1000
Aqua-Poly/Mount	Polysciences, Inc	Cat#18606
Corning Matrigel Basement Membrane Matrix	Sigma	Cat#CLS354234
Trypsin from bovine pancreas	Sigma	Cat#T9935
Deoxyribonuclease I from bovine pancreas	Sigma	Cat#D5025-375KU
Transferrin	Calbiochem	Cat#616420
Cytosine Arabinoside (Ara-C)	Sigma	Cat#C6645
Tetrodotoxin (TTX)	Enzo Life Sciences	Cat#BML-NA120-0001
D(−)-2-Amino-5-phosphonopentanoic acid (AP-5)	Sigma	Cat#A8054
Picrotoxin (PTX)	Sigma	Cat#P1675
(+)-Bicuculline	Sigma	Cat#14340-25MG
DREADD agonist 21 (Compound 21) dihydrochloride (water soluble)	HelloBio	Cat#HB6124
8-(4-Chlorophenylthio)adenosine 3′,5′-cyclic monophosphate (C-CPT-cAMP), Cell permeable cAMP analog	Abcam	Cat#93882-12-3
cAMPS-RP, triethylammonium salt	Tocris	Cat#1337
KT 5720, selective protein kinase A inhibitor	Tocris	Cat#1288
Citral	Sigma	Cat#83007
NASPM trihydrochloride	Tocris	Cat#27-661-0
MEM: Minimum Essential Medium	Gibco	Cat# 51200-038
Sodium bicarbonate	Sigma	Cat#56297-250G
Sodium Chloride	Sigma	Cat#S9888-1KG
Insulin	Sigma	Cat#10516
D-(+)-Glucose	Sigma	Cat#G8270-1KG
Critical commercial assays		
ProFection Mammalian Transfection System	Promega	Cat#E1200
Experimental models: Organisms/strains		
Sprague-Dawley rats, CD1	Charles River	Strain code: 400

(*Continued on next page*)

Continued

REAGENT or RESOURCE	SOURCE	IDENTIFIER
Recombinant DNA		
pFSW-hGi-Y113C/A203G-mCherry	Generated in lab	N/A
pFSW-EmptyVector-mCherry	Generated in lab	N/A
pRSV-Rv	Didier Trono	Addgene; 12253-Plasmid
pMDLg/pRRE	Didier Trono	Addgene; 12251-Plasmid
pMD2.G	Didier Trono	Addgene; 12259-Plasmid
Software and algorithms		
Prism 8	Prism 8	https://www.graphpad.com/
Fiji	Schindelin et al.[47]	https://imagej.net/software/fiji/downloads
Clampfit	Molecular Devices	https://www.moleculardevices.com
MiniAnalysis	Synaptosoft	https://www.synaptosoft.com/MiniAnalysis

RESOURCE AVAILABILITY

Lead contact

Further information and requests for resources and reagents should be directed to and will be fulfilled by the Lead Contact, Ege T. Kavalali (ege.kavalali@vanderbilt.edu).

Materials availability

We generated two plasmids for this manuscript, pFSW-hGi-Y113C/A203G -mCherry and pFSW-EmptyVector-mCherry, based on pAAV-hSyn-DIO-hM4D(Gi)-mCherry available on Addgene. All plasmids used in the present manuscript will be available via Addgene.

Data and code availability

- All data supporting the findings of this study are included as a Source Data file but can also be shared by the lead author Ege T. Kavalali upon request.
- No original code has been generated in this study.
- Any additional information required to reanalyze the data reported in this paper is available from the lead contact upon request.

EXPERIMENTAL MODEL AND STUDY PARTICIPANT DETAILS

Animals

Sprague-Dawley rat pups of either sex were used for the rat hippocampal cultures. Pregnant Sprague-Dawley rats (Charles River) were housed individually until they gave birth to a litter. All animal procedures were performed in accordance with the guide for the care and use of laboratory animals and were approved by the Institutional Animal Care and Use Committee at Vanderbilt University. Health status of the live animals were periodically checked and confirmed by the veterinary staff of animal facilities of the Vanderbilt University.

Primary hippocampal culture preparation

Hippocampal cultures from Sprague-Dawley rats were generated from postnatal day 1–3 male and female pups and plated on Matrigel coated coverslips as previously described.[48] Briefly, hippocampi were dissected in 20% FBS containing Hank's balanced salt solution, and were washed and treated with 10 mg/mL trypsin and 0.5 mg/mL DNAse at 37°C for 10 min. Tissue was washed again, dissociated with a P1000 tip, and centrifuged at 1200 rpm for 10 min at 4°C. Cells were then resuspended and plated on Matrigel-coated glass coverslips in 24-well plates at a density of six coverslips per hippocampus. Cultures were kept in humidified incubators at 37°C for and gassed with 95% air and 5% CO2. Plating media contained 10% fetal bovine serum (FBS), and 20 mg/L insulin, 2 mM L-glutamine, 0.1 g/L transferrin, 5 g/L D-glucose, 0.2 g/L NaHC03 in minimal essential medium (MEM). After 24h, plating media was exchanged for growth media containing 4 μM cytosine arabinoside (as well as 5% FBS, 0.5 mM L-glutamine, and B27) to inhibit glial proliferation. On day *in vitro* (DIV) 4, growth media was exchanged to a final concentration of 2 μM cytosine arabinoside. For lentiviral gene expression, neurons were infected with the lentivirus containing our plasmid of interest at DIV 4. For neurons that underwent sparse transfection experiments, transfection was performed on DIV 7 (See below).

METHOD DETAILS

Sparse neuron transfection

Neuronal sparse transfections were performed on DIV 7 using a Ca2+ phosphate kit (ProFection Mammalian Transfection System, Cat #E1200, Promega), based on a previously described method.[49] A DNA/calcium phosphate mixture was prepared as follows (per well/24-well plate): 1 μg of plasmid DNA, 2 μL of 2M CaCl2, and 15 μL dH2O. This mixture was then added dropwise to an equal volume of 23 N-2-Hydroxyethylpiperazine-N0 -2-Ethanesulfonic Acid (HEPES), while constantly low-vortexing between drop addition. The combined solution was allowed to form for 15 min at room remperature. Neuron conditioned media (1mL/well) was saved and replaced with warmed MEM, and 30 μL of plasmid mixture was added dropwise to each well. Plates were returned to 5% CO2 incubator at 37°C for 30 min, followed by washing the cells twice with 1mL MEM, after which previously saved conditioned media was added back to each well. Neurons were used for experiments at DIV 15–18.

Immunocytochemistry and imaging

To quantify pyramidal neurons expressing viral transfection of pFSW-hGi-Y113C/A203G -mCherry, we stained against mCherry (fluorescence marker for hM4D(Gi)) and MAP2. Cultures were fixed with 4% paraformaldehyde (PFA) and 4% sucrose in phosphate-buffered saline (PBS) at room temperature for 15 min. After three washes, cells were blocked using a solution consisting of 1% bovine serum albumin (BSA) and 2% goat serum was added for 1–2 h. Primary antibody diluted in blocking solution was added and incubated overnight at 4°C in a humid chamber: 1:200 anti-mCherry (M11217, Thermo Fisher). Neuron cultures were washed three times with PBS then refixed with 4% paraformaldehyde (PFA) and 4% sucrose in phosphate-buffered saline (PBS) at room temperature for 15 min. After three washes, cells were permeabilized for 30 min with 0.2% Triton X- in PBS. Coverslips were washed three times with PBS and primary antibody was added and incubated overnight at 4°C in a humid chamber: 1:500 anti-MAP2 (188004, Synaptic Systems). The following day, coverslips were washed three times then incubated with species appropriate Alexafluor secondary antibodies for 90 min at room temperature. Coverslips were then washed and mounted on glass slides using aqua-polymount and imaged using a Zeiss LSM 510 META confocal microscope (CarlZeiss, Oberkochen, Germany). For confocal images, Z-stacks were collected using 63x (NA1.4) oil objective.

Drug treatment

Compound 21 (CMPD21, Hello Bio, Bristol, UK) was fully dissolved in DMSO for 1mM stock and kept at −20°C before testing. Primary hippocampal cultures were treated with 1μM CMPD21 for 48 h before electrophysiology. Control samples were treated with the equivalent volume of DMSO for the respective amount of time. No drugs were present in the bath solution for any electrophysiology experiments, unless otherwise stated.

AM580 (Cayman, Ann Arbor, MI, USA) was fully dissolved in DMSO for 5mM stock and kept at −20°C before testing; cultures were treated with 5μM AM580 for 1 h before electrophysiology experiments. 8-CPT (Abcam, UK) was fully dissolved in H2O for 1mM stock and kept at −20°C then brought to RT for 1 h before testing; cultures were treated with 1μM 8-CPT for 48 h before electrophysiology.

cAMPS-RP (Tocris, Bristol, UK) was solubilized in H2O for 1mM stock and kept at −20°C before testing; cultures were treated with 10μM cAMPS-RP for 48 h before electrophysiology. Citral (St. Louis, MO, USA) was fully dissolved in DMSO for 1mM stock and kept at −20°C before testing; whenever 5 μM Citral was co-applied on cultures, treatment began 24 h before electrophysiology experiments. KT5720 (Tocris, Bristol, UK) was solubilized in DMSO for 1mM stock and kept at −20°C; 1μM KT5720 was applied to cultures for 48 h prior to electrophysiology experiments.

NASPM trihydrochloride (Tocris, Bristol, UK) was solubilized in H2O for 50mM stock and kept at −20°C before testing. Whenever 50μM NASPM trihydrochloride was applied in electrophysiology, cultures were treated with acute bath perfusions following chronic treatment with various drugs (described previously.).

Electrophysiology

Whole-cell patch clamp recordings were performed on pyramidal neurons at DIV14-21 at a clamped voltage of −70 mV. For current clamp experiments, no current was injected. All acute treatment recordings were performed following a 2 min equilibration period after perfusion. Recordings were 3–5 min in length. All recordings were performed using a Burleigh PCS-5000 headstage, Axopatch 200B amplifier, Digidata 1550B digitizer, and Clampex 11.1 software (Molecular Devices). Action potentials were analyzed using Clampfit 11.1 software and mEPSCs were analyzed using MiniAnalysis software (Synaptosoft). Internal pipette solution contained 115 mM CsMeSO3, 10 mM CsCl, 5mM NaCl, 10 mM HEPES, 0.6 mM EGTA, 20 mM tetraethylammonium chloride, 4 mM Mg-ATP, 0.3 mM Na3GTP, pH 7.3–7.3, 10 mM QX-314 [N-(2,6-dimethylphenyl-carbamoylmethyl)-triethylammonium bromide]. The extracellular Tyrode's solution contained 150 mM NaCl, 4mM KCl, 2 mM CaCl2, 10 mM glucose, and 10 mM HEPES (pH7.4), 308 mOsm. To isolate AMPA-mediated mEPSCs, 1μM TTX, 50 μM AP-5 and 50 μM PTX (or 50 μM Bicuculline) were included in the bath. For current clamp experiments, no drugs were included in the bath solution, unless otherwise noted. Internal pipette solution for current clamp experiments was the same but included K-Gluconate and excluded CsCl, CsMeSO3, and QX-314.

QUANTIFICATION AND STATISTICAL ANALYSIS

Statistical analyses were performed using Prism (GraphPad Software). All data are reported as mean ± SEM. An unpaired two-tailed t test was used for comparison when comparing two groups. For parametric analysis of multiple comparisons, two-way analysis of variance (one-way ANOVA and two-way ANOVA) with Tukey *post hoc* or Dunnett's test were used. For other data, a Kruskal-Wallis test followed by Tukey's *post hoc* correction was used for multiple comparisons. Outliers were identified with Robust regression and Outlier removal (ROUT) method. Differences among experimental groups were considered statistically significant when a p value < 0.5 was reached. Significant symbols used in figures are defined as such: *$p < 0.05$; **$p < 0.01$; ***$p < 0.001$; n.s. The number of neurons for each experiment are given in the figure legends, and individual data points represent neurons unless indicated otherwise.